Removal of Ca^{2+}, Mg^{2+}, Ba^{2+} and Sr^{2+} from shale gas flowback water from the Sichuan Basin in China by chemical softening under the guidance of OLI Stream Analyzer: precipitation behaviors and optimization study

Wenshi Liu, Lingru Sun and Sha Tao

ABSTRACT

The disposal of flowback water is recognized as a key issue for the sustainable shale gas development and discharge after reasonable treatment is considered as a feasible pathway. One of the challenges during treatment is the severe mineral scaling potential in reverse osmosis desalination, especially with high amounts of Ca^{2+}, Mg^{2+}, Ba^{2+} and Sr^{2+} in flowback water. In this study, precipitation behaviors of Ca^{2+}, Mg^{2+}, Ba^{2+} and Sr^{2+} during traditional chemical softening was evaluated so as to achieve optimal chemical dosage. Both jar tests and OLI Stream Analyzer simulation revealed that the main precipitates were $CaCO_3$, $SrCO_3$ and $BaSO_4$ during Na_2CO_3 addition, and Ba^{2+} could not be removed efficiently by Na_2CO_3 unless a high dosage was applied since Ba^{2+} would react after the precipitation of Ca^{2+} and Sr^{2+}. Reverse Osmosis System Analysis simulation indicated that Ba^{2+} was a concern because Ba^{2+} would form tenacious $BaSO_4$ scale on the reverse osmosis membranes. Finally, the Na_2SO_4-NaOH-Na_2CO_3 process was proposed for chemical softening as it has a high removal efficiency and low chemical cost. Overall, this study presents an effective chemical softening method and OLI Stream Analyzer could serve as a reliable tool for the calculation, which would finally improve the design and operation of shale gas flowback water treatment.

Key words | chemical softening, coprecipitation, flowback water, OLI Stream Analyzer, shale gas

Wenshi Liu (corresponding author)
Lingru Sun
Sha Tao
School of Chemistry and Chemical Enginerrring,
Southwest Petroleum University,
Chengdu 610500,
China
E-mail: *liuwenshi@swpu.edu.cn*

HIGHLIGHTS

- High concentration of Ba^{2+} in shale gas flowback water should be considered in chemical softening.
- Na_2SO_4-NaOH-Na_2CO_3 was an effective chemical softening process with high Ba^{2+} removal efficiency and low chemical cost.
- OLI Stream Analyzer could provide reliable guidance on chemical softening.

INTRODUCTION

Technically, the global recoverable shale gas is 214.5 trillion cubic meters, meaning it could be an alternative to conventional natural gas in the future (UNCTAD 2018). The USA was the first country to develop shale gas, and in 2018, its total production of shale gas reached 625.8 billion cubic meters, accounting for 60% of the total domestic production of natural gas (EIA 2019). The US shale gas boom has fueled the ambitions of the oil and gas industry in China, with the first shale gas well fractured successfully in 2010, which thus marked the beginning of the shale gas industry in China. Currently, as one of four countries to commercialize shale gas, China is the second-largest shale gas producer in the world, producing 10.8 billion cubic meters in 2018.

doi: 10.2166/wst.2020.355

In China, especially in the Longmaxi Formation in the Sichuan Basin, the water consumption of fracturing fluid used in a single well is about 16,000–40,000 m^3. About 10–20% fracturing fluid is sent back to the ground in four weeks, while the remaining water will flow back as a gas-water mixture with daily water production of 1–10 m^3/d at the later stage. Generally, the flowback water (FBW) contains a variable composition of pollutants, including high salinity, suspended solids, organic chemicals, heavy metals, and naturally occurring radioactive materials (NORMs), making it hard to purify from the perspective of wastewater treatment (Gregory *et al.* 2011).

Traditionally, particularly in the early stage of exploitation, recycling is the main disposal method (Butkovskyi *et al.* 2017). However, once fracturing halts, recycling is not feasible. In addition, environmental regulations might hinder the application of deep well injection (Estrada & Bhamidimarri 2016), and sometimes the transportation distance is long, resulting in a high cost of wastewater disposal. Hence, discharge has gained more attention as a feasible pathway for operators and academic researchers (Nasiri *et al.* 2017). In the process proposed for discharging, the key technology is assumed to be desalination, whose difficulties and cost increase with the elevation of total dissolved solids (TDS) (Onishi *et al.* 2017). It is reported that reverse osmosis (RO) works well when TDS content of the FBW is below 40,000 mg/L, and mechanical vapor recompression (MVR) performs better when TDS is over 40,000 mg/L (Gregory *et al.* 2011). Considering that the TDS in FBW from the Sichuan Basin is usually less than 40,000 mg/L, RO should be the core desalination process. However, the scaling risks cannot be avoided with RO. Potential scale, such as calcium, magnesium, barium, and strontium minerals, might hinder the achievement of maximum processing potential (Mohammadesmaeili *et al.* 2010). Therefore, it is crucial to set up the correct softening pretreatment in order to guarantee the efficiency and continuity of the desalination process.

Water softening, often called hardness removal, is usually performed by chemical precipitation, electrochemical precipitation, cation ion exchange, and nanofiltration (NF). In recent years, electrochemical precipitation has been studied a lot, including multistage electrochemical precipitation, paired electrolysis, and electrodialysis reversal (Lee *et al.* 2013; Yu *et al.* 2018; Sanjuán *et al.* 2019). However, their efficiency does not achieve a satisfactory level in actual wastewater, and energy consumption is also quite high. At the same time, Dong *et al.* (2016) applied cation ion exchange to remove over 98% Ca^{2+} in artificial water. Other methods, including modified ion exchange and combination processes like ultrasound-cation ion exchange, have also been employed to remove hardness (Entezari & Tahmasbi 2009; Mautner *et al.* 2019). However, the application of ion exchange in very hard water will increase backwash times, which may shrink the life cycle of resins. Modified NF has been studied to remove divalent ions Mg^{2+} (Liu *et al.* 2015; Das *et al.* 2019), which all neglect the membrane pollutants such as scale ions Ca^{2+}, Ba^{2+}, Sr^{2+}, and organics in real complex water. Chemical precipitation is well-used because of its low cost and easy availability, especially in very hard and high TDS water. Hence, chemical precipitation was selected as the pretreatment for FBW disposal. Generally, hardness removal focuses on Ca^{2+} and Mg^{2+} and therefore neglects their group members Ba^{2+} and Sr^{2+}, whose minerals also contribute to scaling (Esmaeilirad *et al.* 2015). Since the quality of FBW always varies with the flowback time, the concentration of hardness ions changes as well. Simulation software can simulate the change tendency of ions and provide guidance on economical reagent addition schemes. However, the complete simulation and process schemes of softening for variable water quality have rarely been reported.

Hence, the focus of this study was on the pretreatment optimization and precipitation behaviors of Ca^{2+}, Mg^{2+}, Ba^{2+} and Sr^{2+} based on typical FBW in the Sichuan Basin. OLI Stream Analyzer was used to simulate chemical softening and to provide a suggestion on pretreatment optimization. Jar tests were conducted to verify the accuracy of the simulation and to investigate the precipitation behaviors of Ca^{2+}, Mg^{2+}, Ba^{2+} and Sr^{2+}. A chemical softening procedure was given.

MATERIALS AND METHODS

FBW characteristics

The water samples were taken from a shale gas well (Sichuan Province, China) and collected in 25 L plastic containers until the containers were full. The containers were then sealed until the experiments were carried out to prevent CO_2 from escaping. Prior to each experiment, the plastic container was shaken for several minutes until the particles and sediments in it were re-suspended in the water. The key characteristics of this water are shown in Table 1. In order to eliminate the suspended solids and oil and grease, pre-coagulation was applied. Based on previous

Table 1 | Characterization of shale gas flowback water

Analyte	Result	Analyte	Result
pH	6.50	S^{2-} (mg/L)	N.D.
TSS (mg/L)	95	TDS (mg/L)	30,972
NH_3-N (mg/L)	49	Alkalinity (mg/L)	335.33
Turbidity	178.2	COD (mg/L)	3,582
K^+ (mg/L)	258.8	TOC (mg/L)	13.57
Ca^{2+} (mg/L)	370.25	Na^+ (mg/L)	12,535
Ba^{2+} (mg/L)	141.9	Mg^{2+} (mg/L)	65.555
Fe (mg/L)	N.D.	Sr^{2+} (mg/L)	68.945
B (mg/L)	28.52	Si (mg/L)	30.297
Br^- (mg/L)	82.34	Cl^- (mg/L)	15,042.32
SO_4^{2-} (mg/L)	29.36	F^- (mg/L)	16
Oil and grease (mg/L)	4.15	NO_3^- (mg/L)	32.88
Ionic strength (M)	0.52		

experiments, the process was as follows: coagulation with 50 mg/L ferric chloride (analytical grade, Cologne Chemicals co. Ltd., China) at a rate of 800 sec^{-1} velocity gradient for 1 min; flocculation with 6 mg/L anionic polyacrylamide solution (10 million molecular weight, Cologne Chemicals Co. Ltd., China) at a rate of 40 sec^{-1} velocity gradient for 20 min. After settling for 30 min, the supernatant was filtered through a 0.45 μm nylon filter membrane. The main cations and anions remained basically the same as in the raw water.

Simulation tools

MINEQL+, PHREEQC and OLI Stream Analyzer are widely used for chemical equilibrium calculation. The difference between them is the activity-ionic strength models they apply. The activity-ionic strength models can be divided into ion-association models and ion-interaction models. The main ion-association models are listed in Table 2.

For all equations shown in Table 2, μ is ionic strength and a_i and b_i are parameters determined by the ion size, while A and B are temperature-related factors.

The most commonly used ion-interaction model is the semi-empirical Pitzer equation based on statistical mechanics, assuming all charged ions are independent individuals with electrostatic interaction and short-range interaction. Due to the complexity of the system, the calculation procedure is complicated to carry out manually. MINEQL+ uses the Davis equation to calculate the activity coefficient, which means the software is available when the

Table 2 | Ion-association models (Li 2011)

Models	Equations	Ranges
Debye-Hückel limiting-law equation	$\log(\gamma_i) = -A \cdot Z_i^2 \cdot \sqrt{\mu}$	$\mu < 0.005$
Extended Debye-Hückel equation	$\log(\gamma_i) = \frac{-A \cdot Z_i^2 \cdot \sqrt{\mu}}{1 + B \cdot a_i \cdot \sqrt{\mu}}$	$\mu < 0.01$
Güntelberg equation	$\log(\gamma_i) = -0.5 \cdot Z_i^2 \frac{\sqrt{\mu}}{1 + 1.4 \cdot \sqrt{\mu}}$	$\mu < 0.01$
Davis equation	$\log(\gamma_i) = -A \cdot Z_i^2 \left(\frac{\sqrt{\mu}}{1 + \sqrt{\mu}} - 0.2\mu \right)$	$\mu < 0.5$
Wateq Debye-Hückel equation	$\log(\gamma_i) = \frac{-A \cdot Z_i^2 \cdot \sqrt{\mu}}{1 + B \cdot a_i \cdot \sqrt{\mu}} + b_i \cdot \mu$	$\mu < 1$

ionic strength does not exceed 0.5 molality. Only below the limits can the model give accurate results, but clearly, the ionic strength of the water samples exceeds the limit. Thus, it was not suitable for this study. PHREEQC, a hydrogeochemistry calculation software developed by the United States Geological Survey (USGS), was embedded in the Pitzer model in version 3.0, making it possible to apply in a high ionic strength solution. The OLI Stream Analyzer software, developed by OLI Systems Inc., uses the Debye-Hückel model and the Pitzer model and is widely applied in the petrochemical industry. In the Sichuan Basin, the TDS of FBW is lower than 40,000 mg/L, corresponding to the ionic strength of less than 1 M, thus it is not possible to apply PHREEQC. Besides, TDS changes with flowback time, which requires a wider adaption of software. OLI Stream Analyzer software with both ion-association and ion-interaction model databases has already been proven to be a good fit for the oil and gas industry (Yang 2014). Hence, OLI Stream Analyzer software was selected to simulate the softening process in this study.

Jar tests

Batch studies were performed using a series of jar tests to simulate chemical softening treatment (i.e., rapid mix, sedimentation and filtration). An MY3000-6 series six-paddle standard jar-tester (Meiyu Instruments co., Ltd, Wuhan, China) was used to perform all jar-testing experiments. All experiments were conducted at room temperature (20 °C).

NaOH: precipitation behaviors of FBW were studied in 1 L beakers. The contents of the beaker were completely mixed with paddles. The jar test paddles were run at a rate of 800 sec^{-1} velocity gradient to simulate a rapid mix. 1 mol/L NaOH (analytical grade, Cologne Chemicals Co., Ltd., China) was prepared. Based on the simulations, the

dosages of NaOH from 200 to 800 mg/L at intervals of 100 mg/L were added and allowed to rapid mix for 90 min to ensure sufficient reaction. After rapid mixing, it took 30 min for the sediments to settle and the pH to stabilize. The supernatant was filtered through 0.45 μm nylon filter membranes and immediately acidified to pH < 3 with HNO_3 (1:1, analytical grade, Cologne Chemicals Co., Ltd., China). The water samples were immediately analyzed to avoid further reaction.

***Na_2CO_3*:** 0.5 mol/L Na_2CO_3 (analytical grade, Cologne Chemicals Co., Ltd., China) was prepared. Based on the simulations, 500, 1,000, 2,000, 3,000, and 4,000 mg/L dosages of Na_2CO_3 were added. The procedure was the same as above.

***Na_2SO_4*:** 1 mol/L Na_2SO_4 (analytical grade, Cologne Chemicals Co., Ltd., China) was prepared. Based on the simulations, 50, 100, 150, 200 and 300 mg/L dosages of Na_2SO_4 were added. The procedure was the same as above.

***NaOH-Na_2CO_3 process*:** pretreatment optimization studies were also conducted in 1 L beakers. According to the comparison of simulation and experiments, 1 mol/L NaOH with 700 mg/L was the optimum addition. In view of this, 500, 1,000, 1,500, 2,000 and 3,000 mg/L dosage of Na_2CO_3 were then added. The procedure was the same as above.

***Na_2SO_4-NaOH-Na_2CO_3 process*:** based on the simulations and experiments, 1 mol/L Na_2SO_4 with 100 mg/L and 1 mol/L NaOH with 700 mg/L were the optimum additions. In view of this, 500, 1,000, 1,500, 2,000 and 3,000 mg/L dosages of Na_2CO_3 were then applied. The procedure was the same as above.

The cations were analyzed using an inductively coupled plasma optical emission spectrometer (ICP-OES, ICAP 6300, Thermo). Precipitated solids were washed with deionized water (DI water), and dried in an electric oven for subsequent petrographic and morphological characterization. For X-ray diffraction (XRD) analysis, solids were affixed to sample slides and a PANalytical X'Pert Pro Diffractometer (Almelo, the Netherlands) using Cu Kα radiation was utilized to conduct the experiments. Scans were performed over a 2-theta range between 5° and 70°. Pattern analysis was performed using the computer software MDI Jade (Version 6.5). For the scanning electron microscopy (SEM) and energy-dispersive X-ray spectroscopy (EDS) analyses, samples were imaged with a ZEISS EV0 MA15 scanning electron microscope (Carl Zeiss Micrographics Co., Ltd). The typical accelerating voltage was 0.2–30 kV with continuous adjustment. The supporting EDS was used to conduct elemental analysis.

RESULTS AND DISCUSSION

NaOH addition

The solubility product constants (K_{sp}) of possible softening precipitates are listed in Table S1 in the Supplementary Material. Since the K_{sp} of magnesium hydroxide ($Mg(OH)_2$) is only 1.8×10^{-11}, Mg^{2+} would easily form $Mg(OH)_2$ under alkaline conditions. As the raw water was neutral to slightly acidic (pH 6.50), it was necessary to supply alkali to react with Mg^{2+}. According to the simulation of the OLI Stream Analyzer (as shown in Figure 1(a)), dissolved Ca^{2+} and Sr^{2+} continued to decrease with NaOH dosage ranging from 0 to 300 mg/L. The more alkaline the solution was, the higher the amount of HCO_3^- converted to CO_3^{2-} (Silva *et al.* 2019), which would contribute to the formation of calcium carbonate ($CaCO_3$) and strontium carbonate ($SrCO_3$). Once the NaOH dosage increased to over 300 mg/L, the carbonate alkalinity in water had been largely consumed, and the main reaction shifted to the reaction of Mg^{2+} and OH^- corresponding to the increasing NaOH dosage. When the pH was raised to about 11 with the addition of 700 mg/L NaOH, dissolved Mg^{2+} decreased sharply to less than 0.1 mg/L. Also, a comparison of the XRD patterns of the dosages of 200 mg/L and 600 mg/L NaOH (Figure 2) verified that the low content of OH^- could not induce the precipitation of Mg^{2+}, which was consistent with the result of EDS (Figure 3).

The simulation of the OLI Stream Analyzer showed that the concentration of Ba^{2+} decreased by about 28.56% initially but barely changed through the softening process. The precipitate formed was shown to be $BaSO_4$ rather than $BaCO_3$, which was independent of NaOH addition. That could be attributed to the supersaturation of $BaSO_4$ in the raw flowback water (saturation index, SI = 4). As a matter of fact, the solubility of $BaSO_4$ would decrease with the reduction of the temperature and pressure (Moghadasi *et al.* 2003), as the situation when FBW returns to the surface after the hydraulic fracturing, which could easily create the supersaturated state of $BaSO_4$ in the raw flowback water. The metastable state of supersaturated $BaSO_4$ in solution could even reach 6,700 times over the solubility limit (Monnin & Galinier 1988), but it may precipitate after a long period of storage and tests. This phenomenon was confirmed by the XRD and EDS analysis, in which the characteristic peaks of $BaSO_4$ were identified (Figure 2) and elemental Ba was detected (Figure 3), indicating the precipitation of $BaSO_4$.

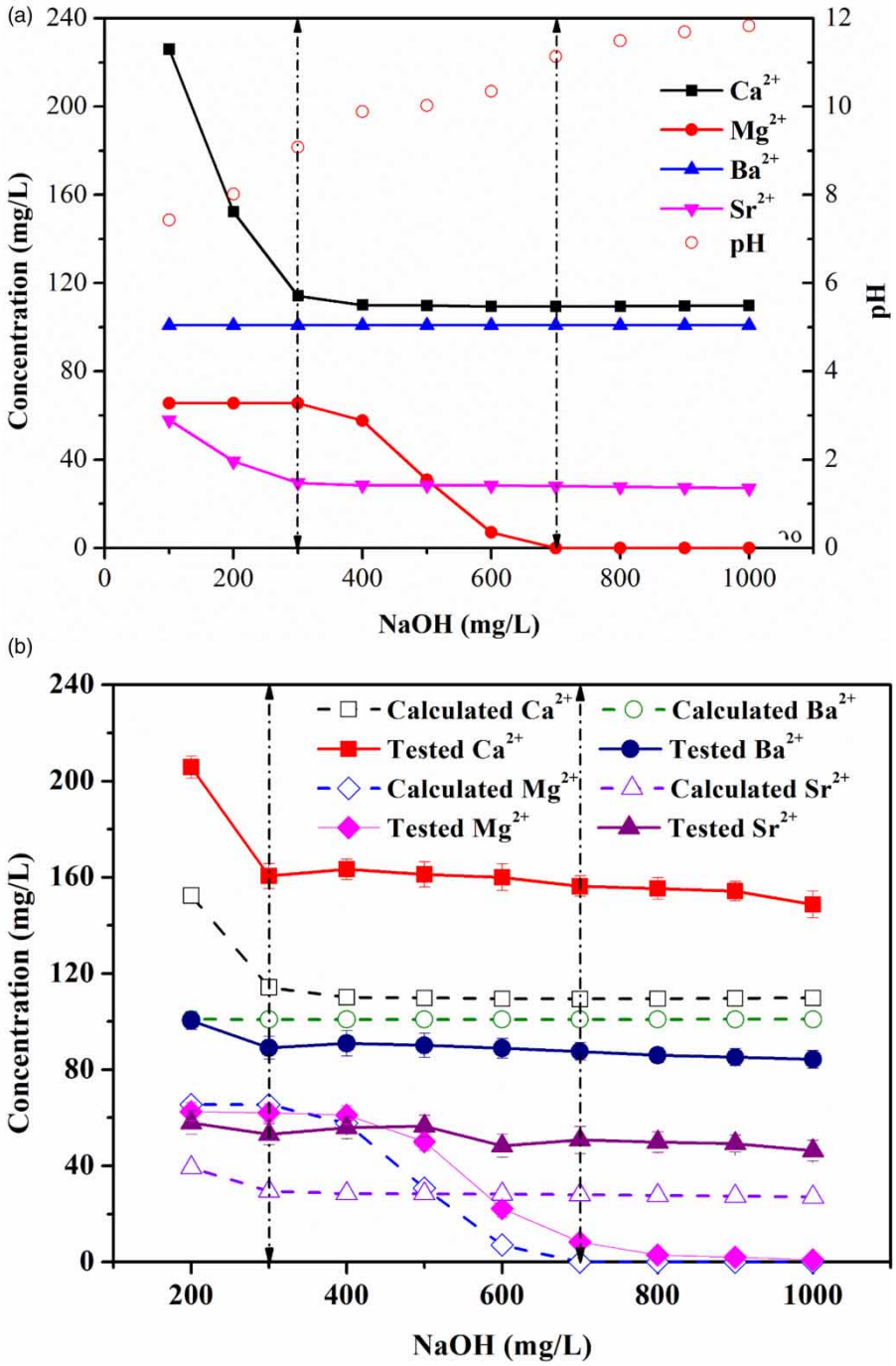

Figure 1 | Under different NaOH dosages (a) the theoretical concentration changes of Ca^{2+}, Mg^{2+}, Ba^{2+}, Sr^{2+} and pH, (b) the comparison of calculated and tested concentrations of Ca^{2+}, Ba^{2+}, $Mg^{2+}$and Sr^{2+}.

At the dosage of 1,000 mg/L NaOH, the removal ratios of Ca^{2+}, Mg^{2+}, Ba^{2+}, and Sr^{2+} were 59.83, 98.46, 40.59 and 32.79%, respectively. As shown in Figure 1(b), the removal ratios of Ca^{2+} and Sr^{2+} in the jar tests were 10.5% and 27.9% lower than the simulation results, while that of Ba^{2+} was 11.72% higher than the simulation, which might be attributed to the coprecipitation mechanism. In tests, because of the similar ionic radii, Ba^{2+} could substitute Ca^{2+} and Sr^{2+} in the lattice of $CaCO_3$ and $SrCO_3$ during precipitation. In Figure 2, the low peak of alstonite

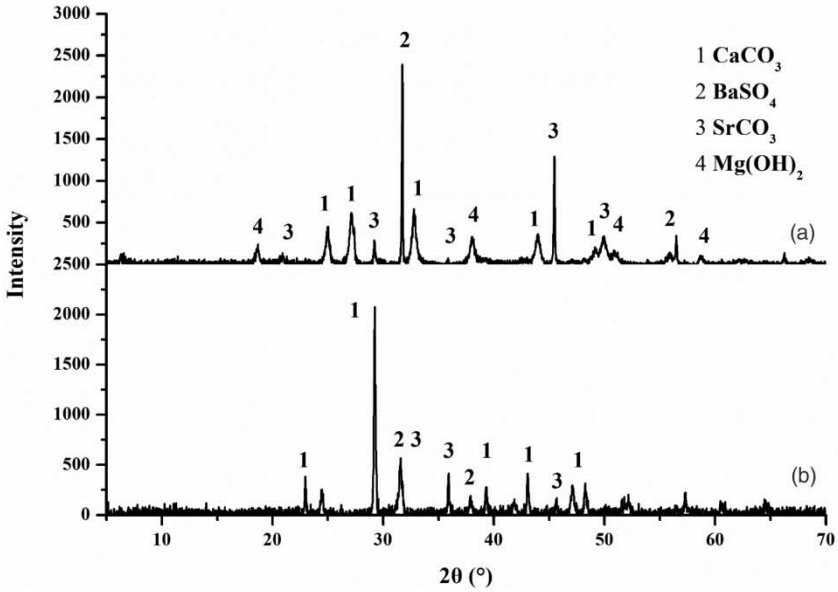

Figure 2 | XRD patterns of solids formed with the NaOH dosages of (a) 200 mg/L, (b) 600 mg/L.

($CaBa(CO_3)_2$) and paralstonite ((Ba, Sr)$Ca(CO_3)_2$) were identified, which indicated the coprecipitation of Ca^{2+}, Ba^{2+} and Sr^{2+}. The presence of soluble Mg^{2+} in the solution could inhibit the precipitation of $CaCO_3$ (Rioyo *et al.* 2018), which might be another explanation for the distinctions of the hardness ion concentration in the jar tests. Since perfect chemical equilibrium was hard to reach during the bench-scale tests, the removal ratios might be lower than expected. Except for $CaBa(CO_3)_2$ and (Ba, Sr)$Ca(CO_3)_2$ formed by coprecipitation mechanism in the jar tests, XRD and SEM/EDS analysis also proved that the simulations could adequately predict the main reaction in water softening (shown in Table 3). The reason for the distinction was that software for chemical equilibrium calculation such as OLI Stream Analyzer are all based on thermodynamic equilibrium, which ignores the kinetics of scale mineral precipitation such as coprecipitation (Bozau & van Berk 2013).

Na_2CO_3 addition

The purpose of adding Na_2CO_3 is to remove noncarbonate hardness. SI (Equation (1)) is always used to reflect the degree of supersaturation of the solution relative to the solid, which determines solid precipitation kinetics as the chemical driving force (Zhang *et al.* 2019). Ca^{2+}, Mg^{2+}, Ba^{2+}, and Sr^{2+} can form similar carbonate precipitates because they are known to be the alkaline-earth metals of Group 2 (IIa) of the periodic table.

$$SI = \log\left[\frac{(M^{2+})(CO_3^{2-})}{K_{sp}(MCO_3)}\right] \quad (1)$$

where the parentheses denote the activity of ionic species, and K_{sp} corresponds to the solubility product. The SI of carbonates are listed in Table S2 in the Supplementary Material.

According to the simulation (Figure 4(a)), because of the low solubility of $CaCO_3$ and $SrCO_3$, Ca^{2+} and Sr^{2+} first decreased to nearly 13.96 mg/L and 3.51 mg/L with the addition of 1,000 mg/L Na_2CO_3. When the dosage changed from 1,000 to 3,000 mg/L, Ba^{2+} began to precipitate from the aqueous phase, leading to the decrease of Ba^{2+} from 100.93 mg/L to about 12.05 mg/L. Finally, Mg^{2+} slightly reduced by 15.99% even when 3,000 mg/L Na_2CO_3 was added, proving that Mg^{2+} could not be removed adequately by only supplying Na_2CO_3. Through the tests, the concentrations of Ca^{2+}, Sr^{2+} and Ba^{2+} were reduced from 370.25 mg/L to 33.83 mg/L, 68.945 mg/L to 28.31 mg/L, and 141.9 mg/L to 8.47 mg/L, respectively. In contrast, only 34.48% of Mg^{2+} was removed. As shown in Figure 4(b), except Mg^{2+}, tested Ca^{2+}, Ba^{2+} and Sr^{2+} concentrations were higher than the values determined by the calculation. Magnesium carbonate minerals always exist as mixed phases, and Mg^{2+} could substitute for Ca^{2+}, Sr^{2+} and Ba^{2+} into the lattice of corresponding carbonate (Thorstenson &

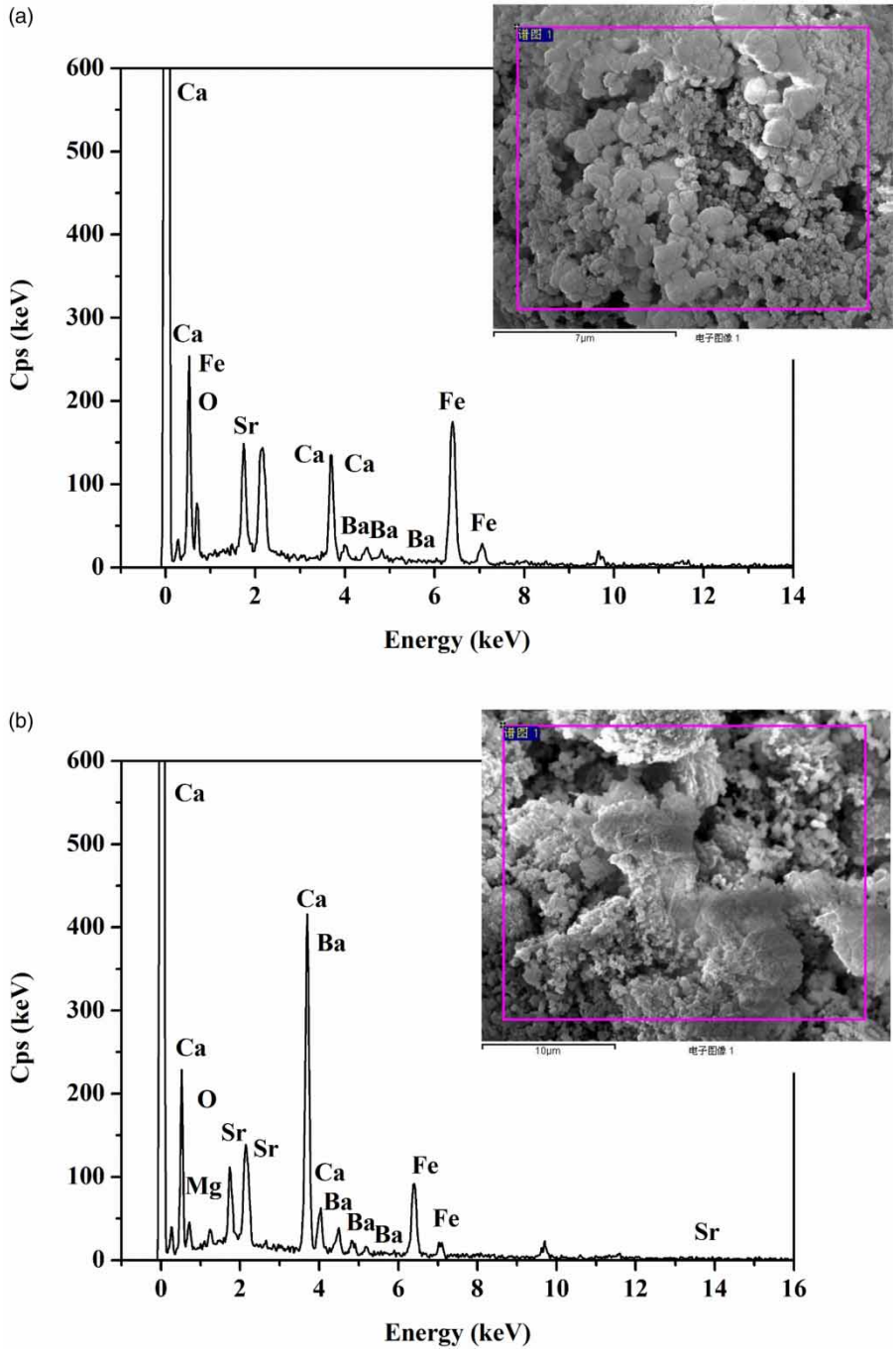

Figure 3 | The SEM/EDS patterns of (a) 200 mg/L NaOH, (b) 600 mg/L NaOH.

Table 3 | Comparison of scale formation between jar tests and simulations

	$BaSO_4$	$CaCO_3$	$SrCO_3$	$Mg(OH)_2$	$CaBa(CO_3)_2$	$(Ba, Sr)Ca(CO_3)_2$
Jar tests	√	√	√	√	√	√
Simulations	√	√	√	√	–	–

√, detected; –, undetected.

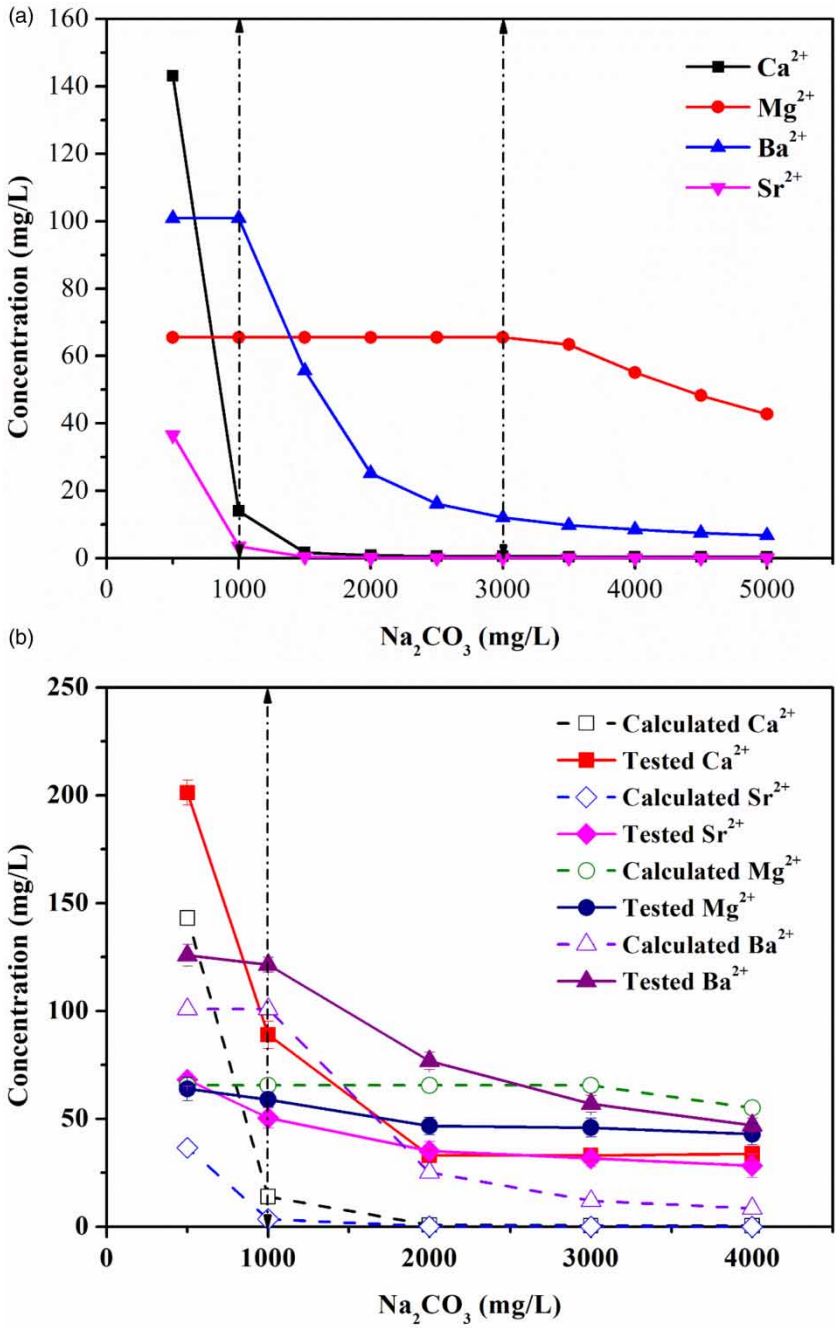

Figure 4 | Under different Na_2CO_3 dosages: (a) the theoretical concentration changes of Ca^{2+}, Mg^{2+}, Ba^{2+}, Sr^{2+}, (b) the comparison of calculated and tested concentrations of Ca^{2+}, Ba^{2+}, Mg^{2+} and Sr^{2+}.

Plummer 1977; Morse *et al.* 2007), which promoted the removal of Mg^{2+}.

Another mechanism that could not be ignored was the salt effect. The high content of NaCl, more than 10,000 mg/L, would strengthen ion-ion interactions and promote solubility (Cao 2007). It might partly explain why Ca^{2+}, Sr^{2+} and Ba^{2+} did not precipitate quantitatively, as demonstrated by the simulation. Coprecipitation would facilitate the precipitation of Mg^{2+} but delay that of other ions, while a salt effect mechanism restrained the removal of all the hardness ions, leading to the higher removal of Mg^{2+} and lower removal of Ca^{2+}, Sr^{2+} and Ba^{2+}.

The XRD patterns (Figure 5) and EDS analysis (Supplementary Material, Figure S1) showed that the Mg

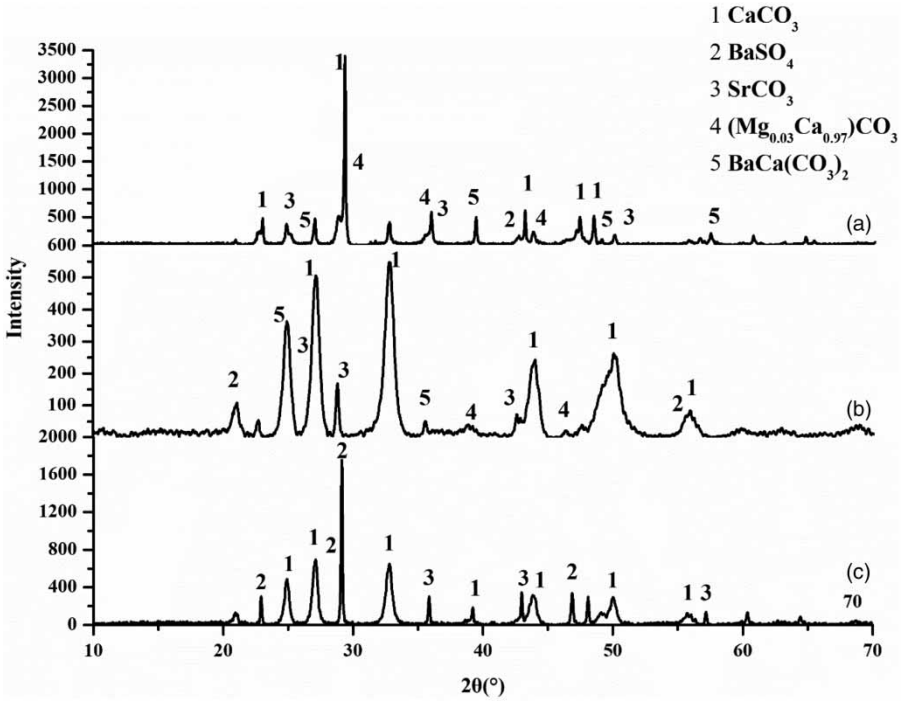

Figure 5 | XRD patterns of solids formed with the Na_2CO_3 dosages of (a) 1,000 mg/L, (b) 2,000 mg/L, (c) 4,000 mg/L.

element appeared in the precipitates when 2,000 mg/L Na_2CO_3 was used, which was earlier than the dosage provided by the simulation (3,000 mg/L), since Mg^{2+} would coprecipitate with Ca^{2+} to form $(Mg_{0.03}Ca_{0.97})CO_3$. Besides, the form of barium-containing precipitates was identified to be $BaCa(CO_3)_2$ instead of $BaCO_3$, verifying the coprecipitation mechanism again. Comparison of the solids formed between jar tests and simulations is presented in Table S3 in the Supplementary Material, which reveals that coprecipitation could be used to explain the inconsistency between the simulations and jar tests.

Na_2SO_4 addition

The significantly higher solubility (3.89 g/100 g, 20 °C) of barium hydroxide as compared to that of magnesium hydroxide (9.628×10^{-4} g/100 g, 20 °C) indicated that it was not a practical way to remove Ba^{2+} from raw water by adding alkali (Esmaeilirad *et al.* 2015). Since $BaSO_4$ is less soluble than other forms of barium, and its precipitation kinetics is quite fast (Zhang *et al.* 2014), it is feasible to apply Na_2SO_4 to precipitate Ba^{2+} in engineering.

According to the simulation results of the OLI Stream Analyzer (Figure 6(a)), Ba^{2+} rapidly decreased to about 0.5 mg/L at the dosage of 300 mg/L Na_2SO_4. Also, Sr^{2+} could combine with CO_3^{2-} and SO_4^{2-} to form solids out of the aqueous phase. However, $BaSO_4$ usually precipitates before the appearance of $SrSO_4$ in the solution when Ba^{2+} and Sr^{2+} coexist, due to the much slower precipitation kinetic of $SrSO_4$ when compared with $BaSO_4$ and Sr^{2+} being likely to coprecipitate with $BaSO_4$ (Zhang *et al.* 2014). Therefore, the main reaction after adding Na_2SO_4 was the $BaSO_4$ precipitation, leading to over 90% removal of Ba^{2+}. Although the concentration of Ca^{2+} remained unchanged, it was slightly lower than that in raw water, which might be attributed to the precipitation of $CaCO_3$. The XRD patterns (Supplementary Material, Figure S2) verified the existence of $CaCO_3$, indicating the supersaturation state of $CaCO_3$ in raw water. Test results showed that a 20.05% decrease of Sr^{2+} still existed, which could be explained by the incorporation of Sr^{2+} into the lattice of $BaSO_4$. Sr^{2+} was prone to coprecipitate with $BaSO_4$, as evidenced by the characteristic peaks of $Ba_{0.75}Sr_{0.25}SO_4$ in the XRD pattern. Nevertheless, as can be seen in Figure 6(b), the removal ratio of Ba^{2+} could reach 99.28% when only 300 mg/L dosage of Na_2SO_4 was used, verifying the high efficiency of Na_2SO_4 to remove Ba^{2+} even with complicated water chemistry in real FBW. The removal ratios of Ca^{2+}, Mg^{2+}, Ba^{2+}, and Sr^{2+} were 12.09, 6.69 99.28 and 20.05%, respectively.

Since both tests and simulation verified that the precipitation of Ba^{2+} would not begin until the residual

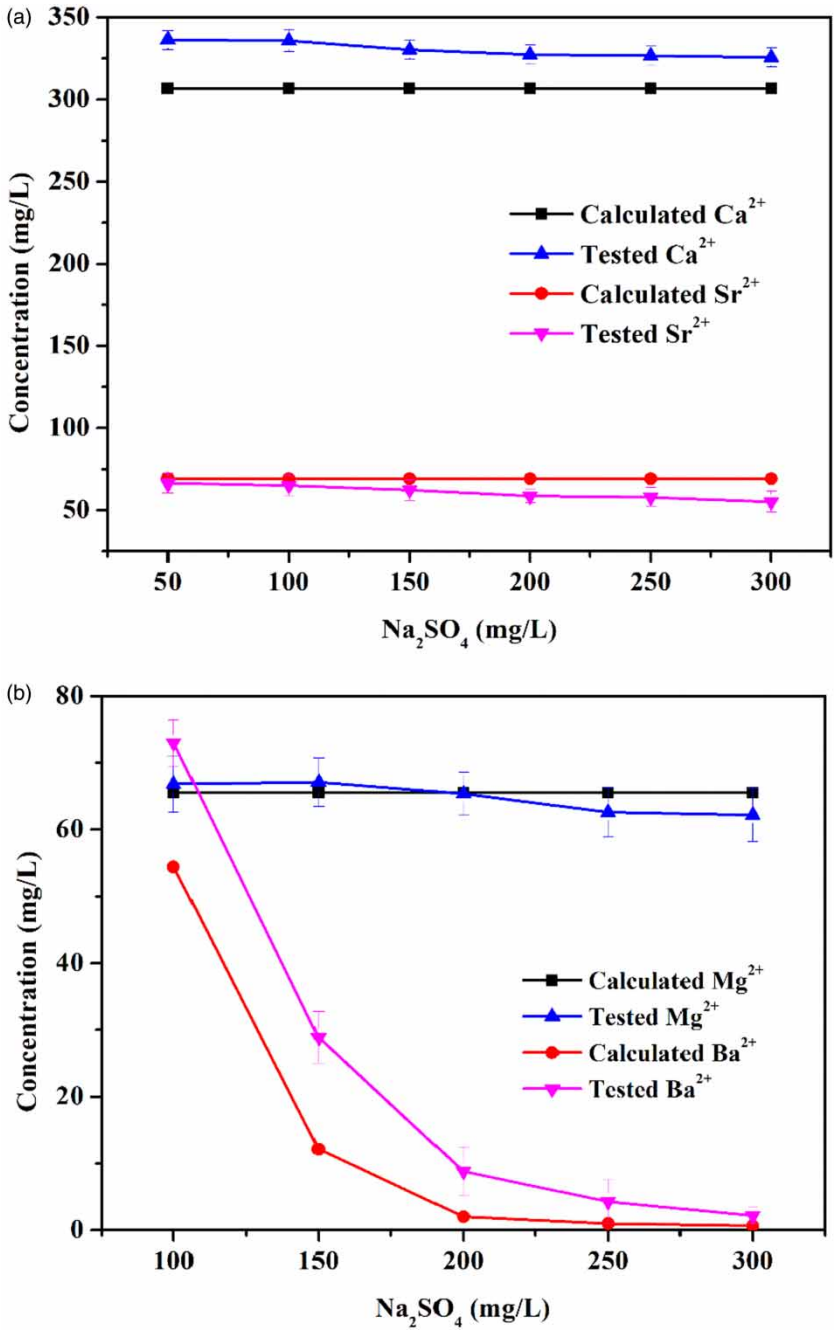

Figure 6 | Under different Na_2SO_4 dosages: (a) the comparison of calculated and tested concentrations of Ca^{2+} and Sr^{2+}, (b) the comparison of calculated and tested concentrations of Ba^{2+} and Mg^{2+}.

concentrations of Ca^{2+} and Sr^{2+} were negligible, the dosage of Na_2CO_3 should be high enough to induce the precipitation of Ba^{2+}. A dosage of up to 4,000 mg/L Na_2CO_3 yielded only 66.81% removal. By contrast, the removal ratio of Ba^{2+} under the application of 300 mg/L $NaSO_4$ could reach 99.28%, which validated the efficiency of adding $NaSO_4$ to remove Ba^{2+} in FBW.

NaOH-Na_2CO_3 process

Since the individual additions could not achieve satisfactory removal efficiency for all hardness ions, as mentioned above, a combinated process was considered. A NaOH-Na_2CO_3 process is often used to induce the precipitation of hardness ions in groundwater (Rioyo *et al.* 2018). Based

on the results in Figure 1, 700 mg/L NaOH was selected as the dosage in the first stage because of the 87.23% removal ratio of Mg^{2+}. This section focuses on the selection of Na_2CO_3 dosage for the second stage. As shown in Figure 7, the removal ratios of Ca^{2+}, Mg^{2+} and Sr^{2+} reached about 97.27, 77 and 65.04%, respectively, when 3,000 mg/L Na_2CO_3 was added after 700 mg/L NaOH. The removal efficiency of Ca^{2+} and Sr^{2+} was 6% higher than with Na_2CO_3 alone. Previous study has shown that the NaOH-Na_2CO_3 process is an effective way to remove calcium and magnesium hardness (Wang *et al.* 2019). However, Ba^{2+} has always been ignored, which might be a cause for $BaSO_4$ scaling, especially in the oil and gas industry (Bageri *et al.* 2017). In fact, even when the Na_2CO_3 dosage was raised to 3,000 mg/L, residual Ba^{2+} was still about 42.5 mg/L. The low removal ratio of Ba^{2+} suggested that the NaOH-Na_2CO_3 process was not suitable for FBW with a high concentration of Ba^{2+}.

Na_2SO_4-NaOH-Na_2CO_3 process

As mentioned above, since 300 mg/L Na_2SO_4 could remove 99.28% of Ba^{2+} in 90 min in the individual process, the Na_2SO_4-NaOH-Na_2CO_3 process was applied. Li (2011) preliminarily verified the feasibility of dosing sulfate and carbonate in the chemical softening process, but there was no specific method in the study. Considering that Ba^{2+} could also be partly removed by coprecipitating with Ca^{2+} and Sr^{2+} through the addition of NaOH and Na_2CO_3, the dosage of 100 mg/L Na_2SO_4 was selected. When the dosage of 2,000 mg/L Na_2CO_3 was added, the concentrations of Ca^{2+}, Mg^{2+}, Ba^{2+}, and Sr^{2+} were reduced to 14.7, 15, 4.43, and 26.1 mg/L, respectively (Figure 8). Through the process, the removal ratio of Ba^{2+} was 31.84% higher than that obtained by the NaOH-Na_2CO_3 process. Further, the market price of Na_2SO_4 is lower than that of Na_2CO_3, meaning that the treatment was both effective and economical.

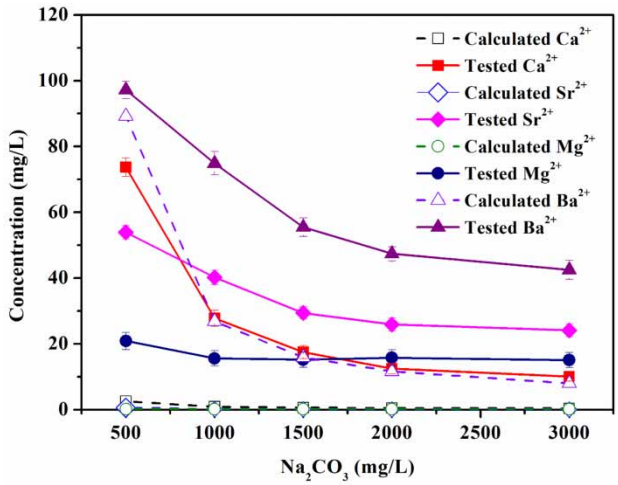

Figure 7 | Under different Na_2CO_3 dosages (after adding NaOH) the the comparison of calculated and tested concentrations of Ca^{2+}, Ba^{2+}, Mg^{2+} and Sr^{2+}.

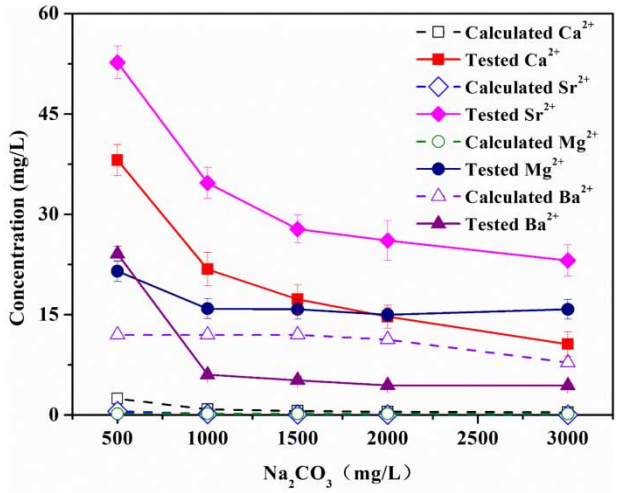

Figure 8 | Under different Na_2CO_3 dosages (after adding NaOH and Na_2SO_4) the comparison of calculated and tested concentrations of Ca^{2+}, Ba^{2+}, Mg^{2+} and Sr^{2+}.

Scaling tendency

The scaling tendency of the FBW was predicted by the Reverse Osmosis System Analysis (ROSA) software (Version 9.0). ROSA software was developed by the Dow Chemical Company to model and predict the performance of RO systems, which is based on empirical data generated by testing FILMTEC™ products at different conditions (Boulahfa *et al.* 2019). As shown in Table 4, the scaling tendency of RO was predicted with FBW as inlet water at various recovery rates. In the table, the Langelier saturation index (LSI) and Stiff & David stability index (S&DSI) were used to evaluate the scaling possibility of $CaCO_3$. If they are greater than 0, the scaling risk of $CaCO_3$ exists. For other mineral scale, there is a risk of scaling if the saturation percentage exceeds 100%. With different recovery rates, LSI was greater than 0, which suggested the possibility of the precipitation of $CaCO_3$. However, more remarkable was the fact that even when $BaSO_4$ saturation far exceeded 100%, the recovery rate was only 10%.

In the operation of RO, pH regulation is often used to control the precipitation of $CaCO_3$, $Mg(OH)_2$, etc. However, it is not effective to prevent the scaling of $BaSO_4$, which can

Table 4 | Scaling tending of inlet water

	Raw inlet water					Pretreated inlet water				
Recovery rates	**10%**	**20%**	**30%**	**40%**	**50%**	**10%**	**20%**	**30%**	**40%**	**50%**
LSI	0.042	0.193	0.364	0.561	0.795	−1.051	−0.900	−0.729	−0.532	−0.298
S&DSI	−0.885	−0.770	−0.643	−0.497	−0.408	−1.959	−1.847	−1.720	−1.573	−1.401
$CaSO_4$ saturation (%)	1.284	0.33	0.38	0.46	0.57	0.00012	0.00013	0.00015	0.00018	0.00023
$BaSO_4$ saturation (%)	7,631	8,696	10,113	12,093	15,065	3.35	3.82	4.43	5.29	6.58
$SrSO_4$ saturation (%)	2.05	2.37	2.79	3.42	4.42	0.0097	0.011	0.013	0.016	0.021
$Mg(OH)_2$ saturation (%)	0.00007	0.00009	0.00014	0.00022	0.00038	0.00003	0.00004	0.00006	0.00009	0.00016

cause flux decline and membrane damage in RO (Boerlage *et al.* 1999). Thus, it is essential to remove Ba^{2+} in the softening process as a pretreatment to desalinate the FBW for the discharge process. After the softening treatment of the Na_2SO_4-NaOH-Na_2CO_3 process with the dosage of 100 mg/L (1 mol/L), 700 mg/L (1 mol/L), and 2,000 mg/L (0.5 mol/L), no scaling tendency was predicted.

CONCLUSION

This study aimed to provide a suitable chemical softening method to prevent mineral scaling in RO desalination during shale gas flowback water treatment prior to discharge. The results showed that high concentrations of Ba^{2+} in flowback water need to be removed during the softening process, since they cause significant $BaSO_4$ scaling. The conventional NaOH-Na_2CO_3 process could precipitate Ca^{2+}, Mg^{2+} and Sr^{2+} effectively, but the removal ratio of Ba^{2+} was limited unless a high dosage of Na_2CO_3 was applied. A small dosage of Na_2SO_4 could lead to a remarkable reduction of Ba^{2+} and also save on Na_2CO_3. OLI Stream Analyzer could predict the precipitation behaviors of Ca^{2+}, Mg^{2+}, Ba^2 and Sr^{2+} in the chemical softening process. This study presents an effective chemical softening method and might provide guidance for shale gas flowback water treatment, which would contribute to suitable shale flowback water solutions and eventual sustainable shale gas development in China.

ACKNOWLEDGEMENT

This work was financially supported by a grant (2015SZ0007) from the Science & Technology Department of Sichuan Province, China, and the Science and Technology Cooperation Project of the CNPC-SWPU Innovation Alliance. The authors gratefully acknowledge PetroChina Company Limited and its branch company PetroChina Southwest Oil & Gasfield Company for financial support and assistance in the fieldwork and simulation.

DATA AVAILABILITY STATEMENT

All relevant data are included in the paper and its Supplementary Information.

REFERENCES

Bageri, B. S., Mahmoud, M. A., Shawabkeh, R. A., Al-Mutairi, S. H. & Abdulraheem, A. 2017 Toward a complete removal of barite (barium sulfate $BaSO_4$) scale using chelating agents and catalysts. *Arabian Journal for Science & Engineering* **42** (4), 1667–1674.

Boerlage, Ś. F., Kennedy, M. D., Witkamp, G. J., van der Hoek, J. P. & Schippers, J. C. 1999 $BaSO_4$ solubility prediction in reverse osmosis membrane systems. *Journal of Membrane Science* **159** (1–2), 47–59.

Boulahfa, H., Belhamidi, S., Elhannouni, F., Taky, M., El Fadil, A. & Elmidaoui, A. 2019 Demineralization of brackish surface water by reverse osmosis: the first experience in Morocco. *Journal of Environmental Chemical Engineering* **7** (2), 102937.

Bozau, E. & van Berk, W. 2013 Hydrogeochemical modeling of deep formation water applied to geothermal energy production. *Procedia Earth and Planetary Science* **7**, 97–100.

Butkovskyi, A., Bruning, H., Kools, S. A., Rijnaarts, H. H. & Van Wezel, A. P. 2017 Organic pollutants in shale gas flowback and produced waters: identification, potential ecological impact, and implications for treatment strategies. *Environmental Science & Technology* **51** (9), 4740–4754.

Cao, Z. 2007 *Study on the Mechanism of Salt Evolution and Scale Formation in Produced Water From High Salinity Oilfield*. PhD Thesis, China university of petroleum, Beijing, China.

Das, R., Kuehnert, M., Sadat Kazemi, A., Abdi, Y. & Schulze, A. 2019 Water softening using a light-responsive, spiropyran-meodified nanofiltration membrane. *Polymers* **11** (2), 344.

Dong, B., Xu, Y., Shen, D., Dai, X. & Lin, S. 2016 Characterizing the interactions between humic matter and calcium ions during water softening by cation-exchange resins. *RSC Advances* **6** (96), 93947–93955.

Energy Information Administration (EIA) 2019 *U.S. Crude Oil and Natural Gas Proved Reserves, Year-End 2018*. Washington, DC.

Entezari, M. H. & Tahmasbi, M. 2009 Water softening by combination of ultrasound and ion exchange. *Ultrasonics Sonochemistry* **16** (3), 356–360.

Esmaeilirad, N., Carlson, K. & Ozbek, P. O. 2015 Influence of softening sequencing on electrocoagulation treatment of produced water. *Journal of Hazardous Materials* **283**, 721–729.

Estrada, J. M. & Bhamidimarri, R. 2016 A review of the issues and treatment options for wastewater from shale gas extraction by hydraulic fracturing. *Fuel* **182**, 292–303.

Gregory, K. B., Vidic, R. D. & Dzombak, D. A. 2011 Water management challenges associated with the production of shale gas by hydraulic fracturing. *Element* **7** (3), 181–186.

Lee, H. J., Song, J. H. & Moon, S. H. 2013 Comparison of electrodialysis reversal (EDR) and electrodeionization reversal (EDIR) for water softening. *Desalination* **314**, 43–49.

Li, M. 2011 *Removal of Divalent Cations From Marcellus Shale Flowback Water Through Chemical Precipitation*. Masters Thesis, University of Pittsburgh, America.

Liu, C., Shi, L. & Wang, R. 2015 Crosslinked layer-by-layer polyelectrolyte nanofiltration hollow fiber membrane for low-pressure water softening with the presence of SO_4^{2-} in feed water. *Journal of Membrane Science* **486**, 169–176.

Mautner, A., Kobkeatthawin, T., Mayer, F., Plessl, C., Gorgieva, S., Kokol, V. & Bismarck, A. 2019 Rapid water softening with TEMPO-oxidized/phosphorylated nanopapers. *Nanomaterials* **9** (2), 136.

Moghadasi, J., Jamialahmadi, M., Müller-Steinhagen, H., Sharif, A., Ghalambor, A., Izadpanah, M. R. & Motaie, E. 2003 Scale formation in Iranian oil reservoir and production equipment during water injection. In: *International Symposium on Oilfield Scale*. Society of Petroleum Engineers.

Mohammadesmaeili, F., Badr, M. K., Abbaszadegan, M. & Fox, P. 2010 Byproduct recovery from reclaimed water reverse osmosis concentrate using lime and soda-ash treatment. *Water Environment Research* **82** (4), 342–350.

Monnin, C. & Galinier, C. 1988 The solubility of celestite and barite in electrolyte solutions and natural waters at 25°C: a thermodynamic study. *Chemical Geology* **71** (4), 283–296.

Morse, W.,J., Arvidson, S. R. & Andreas, L. 2007 Calcium carbonate formation and dissolution. *Chemical Reviews* **204** (8), 990–1005.

Nasiri, M., Jafari, I. & Parniankhoy, B. 2017 Oil and gas produced water management: a review of treatment technologies, challenges, and opportunities. *Chemical Engineering Communications* **204** (8), 990–1005.

Onishi, V. C., Carrero-Parreno, A., Reyes-Labarta, J. A., Fraga, E. S. & Caballero, J. A. 2017 Desalination of shale gas produced water: a rigorous design approach for zero-liquid discharge evaporation systems. *Journal of Cleaner Production* **140**, 1399–1414.

Rioyo, J., Aravinthan, V., Bundschuh, J. & Lynch, M. 2018 Research on 'high-pH precipitation treatment' for RO concentrate minimization and salt recovery in a municipal groundwater desalination facility. *Desalination* **439**, 168–178.

Sanjuán, I., García-García, V., Expósito, E. & Montiel, V. 2019 Paired electrolysis for simultaneous electrochemical water softening and production of weak acid solutions. *Electrochemistry Communications* **101**, 88–92.

Silva, R. D. R., Rodrigues, R. T., Azevedo, A. C. & Rubio, J. 2019 Calcium and magnesium ion removal from water feeding a steam generator by chemical precipitation and flotation with micro and nanobubbles. *Environmental Technology* **40**, 1–20.

Thorstenson, D. C. & Plummer, L. N. 1977 Equilibrium criteria for two-component solids reacting with fixed composition in an aqueous phase e example: the magnesian calcites. *American Journal of Science* **277**, 1203–1223.

United Nations Conference on Trade and Development (UNCTAD) 2018 *Commodities at A Glance: Special Issue on Shale Gas*. United Nations Conference on Trade and Development, New York and Geneva.

Wang, M., Wang, M., Chen, D., Gong, Q., Yao, S., Jiang, W. & Chen, Y. 2019 Evaluation of pre-treatment techniques for shale gas produced water to facilitate subsequent treatment stages. *Journal of Environmental Chemical Engineering* **7**, 1.

Yang, X. 2014 *Precipitation and Removal of Ionic Compounds From Produced Water: Observed Versus Modeling Results*. *Masters Thesis*, Colorado State University, America.

Yu, Y., Jin, H., Quan, X., Hong, B. & Chen, X. 2018 Continuous multistage electrochemical precipitation reactor for water softening. *Industrial & Engineering Chemistry Research* **58** (1), 461–468.

Zhang, T., Gregory, K., Hammack, R. W. & Vidic, R. D. 2014 Co-precipitation of radium with barium and strontium sulfate and its impact on the fate of radium during treatment of produced water from unconventional gas extraction. *Environmental Science & Technology* **48** (8), 4596–4603.

Zhang, P., Zhang, Z., Zhu, J., Kan, A. T. & Tomson, M. B. 2019 Experimental evaluation of common sulfate mineral scale co-precipitation kinetics in oilfield operating conditions. *Energy & Fuels* **33**, 6177–6186.

First received 31 March 2020; accepted in revised form 19 July 2020. Available online 30 July 2020